Geological Magazine

www.cambridge.org/geo

Original Article

Cite this article: Srivastava DC, Goswami A, and Sahay A (2021) Strain-partitioned dextral transpression in the Great Boundary Fault Zone around Chittaurgarh, NW Indian Shield. *Geological Magazine* **158**: 1585–1599. https://doi.org/10.1017/S0016756821000157

Received: 28 October 2020
Revised: 16 February 2021
Accepted: 17 February 2021
First published online: 22 March 2021

Keywords:
Great Boundary Fault; fault core and damage zone; digital elevation model; polyphase folding; en échelon veins; shear zones; Aravalli terrain; Bundelkhand craton

Author for correspondence:
Deepak C. Srivastava,
Email: deepak.srivastava@es.iitr.ac.in

Strain-partitioned dextral transpression in the Great Boundary Fault Zone around Chittaurgarh, NW Indian Shield

Deepak C. Srivastava, Ajanta Goswami and Amit Sahay

Department of Earth Sciences, Indian Institute of Technology Roorkee, Roorkee 247 667, India

Abstract

Delimiting the Aravalli mountain range in the east, the Great Boundary Fault (GBF) occurs as a crustal-scale tectonic lineament in the NW Indian Shield. The structural and tectonic characteristics of the GBF are, as yet, not well-understood. We attempt to fill this gap by using a combination of satellite image processing, high-resolution outcrop mapping and structural analysis around Chittaurgarh. The study area exposes the core and damage zone of the GBF. Three successive phases of folding, F_1, F_2 and F_3, are associated with deformation in the GBF. The large-scale structural characteristics of the GBF core are: (i) a non-coaxial refolding of F_1 folds by F_2 folds; and (ii) the parallelism between the GBF and F_2 axial traces. In addition, numerous metre-scale ductile shear zones cut through the rocks in the GBF core. The damage zone is characterized by the large-scale F_1 folds and the mesoscopic-scale strike-slip faults, thrusts and brittle-ductile shear zones. Several lines of evidence, such as the inconsistent overprinting relationship between the strike-slip faults and thrusts, the occurrence of en échelon folds and the palaeostress directions suggest that the GBF is a dextral transpression fault zone. Structural geometry and kinematic indicators imply a wrench- and contraction-dominated deformation in the core and damage zone, respectively. We infer that the GBF is a strain-partitioned dextral transpression zone.

1. Introduction

Ever since Harland (1971) elucidated transpression in the Caledonian Spitzbergen, a large number of studies have advanced our understanding of the principles governing various transpression types (Sanderson & Marchini, 1984; Fossen & Tikoff, 1993, 1998; Tikoff & Fossen, 1993; Robin & Cruden, 1994; Soto, 1997; Ghosh, 2001; Fossen, 2016). These principles have been successfully tested in many terrains (e.g. Sylvester, 1988; Fossen *et al.* 1994; Tikoff & Teyssier, 1994; Tikoff & Greene, 1997; Dewey *et al.* 1998; Jones *et al.* 2004; Iacopini *et al.* 2008; Cruciani *et al.* 2015; Graziani et al. 2020; Simonetti *et al.* 2020*a*, b). Several landmark contributions on the polyphase folding and strain partitioning in transpression zones have been made during the last couple of decades (e.g. Jones & Tanner, 1995; Allen *et al.* 2001; Tavarnelli *et al.* 2004; Carreras *et al.* 2013; Li *et al.* 2016).

In the NW Indian Shield, the several-hundred-kilometre-long Great Boundary Fault (GBF) has been variously interpreted as a reverse fault, reactivated normal fault or reactivated thrust with occasional references to strike-slip motion (Heron, 1936; Coulson, 1967; Iqbaluddin *et al.* 1978; Prasad, 1984; Verma, 1996; Sinha-Roy *et al.* 1998; Choudhuri & Guha, 2004). The structural geometry and tectonics of the bends in the GBF are not, as yet, addressed. This study focuses on one of the prominent bends in the southwestern part of the GBF around Chittaurgarh, Rajasthan.

2. Geological setting

The NE–SW-trending Aravalli mountain range, a gravity high, occurs as a prominent geomorphic horst in the NW Indian Shield (Mishra *et al.* 2000; Dwivedi *et al.* 2019). Geologically, it is a mosaic that consists of the Aravalli mobile belt, the Delhi mobile belt and vestiges of the basement. The basement, known as the Banded Gneissic Complex (BGC), consists of 2.45–3.5-Ga-old gneisses, granitoids and associated rocks (Sivaraman & Odom, 1982; Gopalan *et al.* 1990; Wiedenbeck & Goswami, 1994; Roy & Kröner, 1996; Wiedenbeck *et al.* 1996). The Aravalli and Delhi mobile belts consist of metasedimentary and meta-igneous assemblages that evolved during the *c.* 2.0–1.8 Ga and *c.* 1.1–0.8 Ga orogenies, respectively (Choudhari *et al.* 1984; Volpe & MacDougall, 1990; Tobisch *et al.* 1994; Wiedenbeck & Goswami, 1994; Deb *et al.* 2001). Table 1 gives a generalized stratigraphy and available radiometric ages of the basement and mobile belts in the Aravalli terrain.

© The Author(s), 2021. Published by Cambridge University Press.

CAMBRIDGE UNIVERSITY PRESS

Table 1. A generalized stratigraphic succession of the Aravalli terrain

Stratigraphy	Age (Ma)	Reference(s)
Synorogenic granites in Delhi Mobile Belt (Delhi Supergroup)	*c.* 1450	Choudhari *et al.* (1984)
Synorogenic granite in Aravalli Mobile Belt (Aravalli Supergroup)	*c.* 1850	Choudhari *et al.* (1984)
Berach, Untala, Ahar, Gingla granitoids	*c.* 2500	Wiedenbeck *et al.* (1996)
Banded Gneissic Complex	*c.* 2600–3300	Gopalan *et al.* (1990), Wiedenbeck & Goswami (1994) and Roy & Kroner (1996)

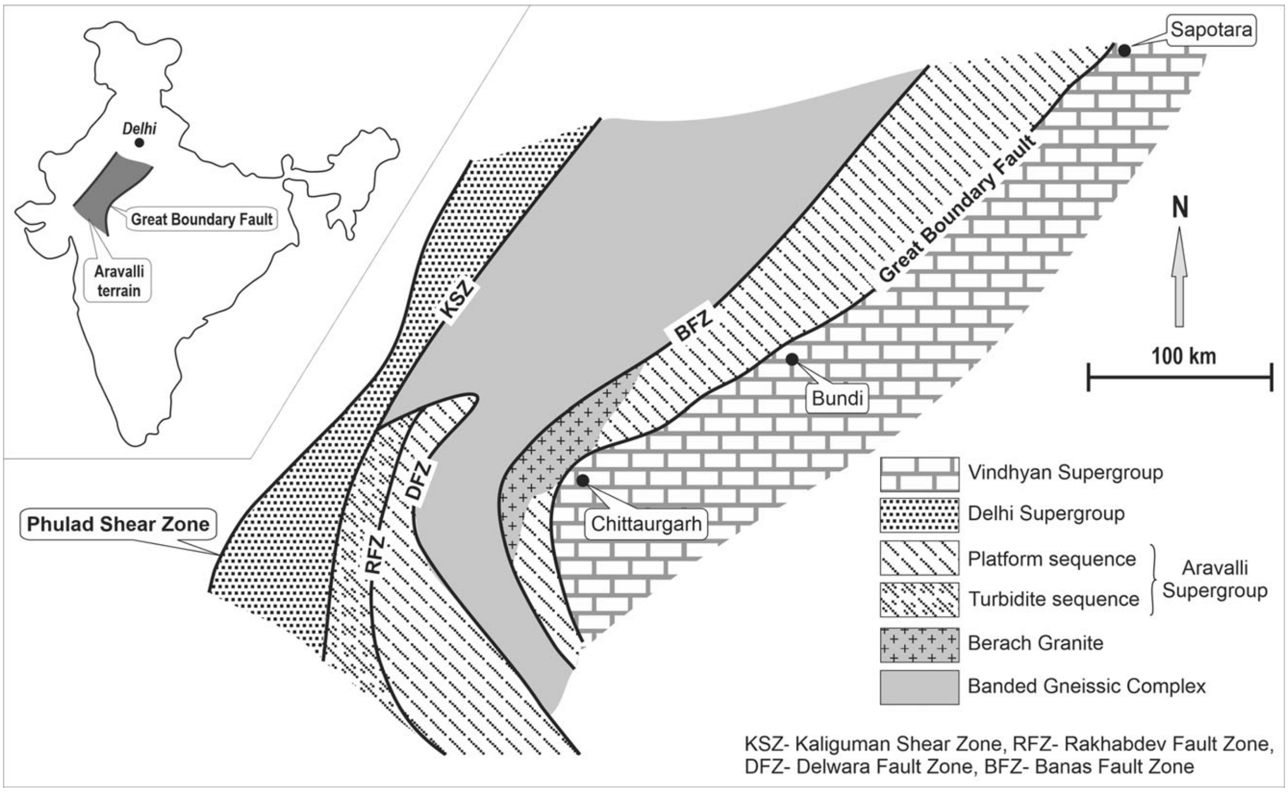

Fig. 1. A simplified geological map of Aravalli terrain showing major tectonic lineaments and different lithounits (after Sinha-Roy *et al.* 1998). Inset shows Aravalli terrain in India.

A series of NE–SW-trending tectonic lineaments, each running for a few hundred kilometres and penetrating up to near Moho depth (*c.* 40 km), cut the Aravalli mountain range in separate blocks (Sinha-Roy *et al.* 1998; Mishra *et al.* 2000; Dwivedi *et al.* 2019). These lineaments occur as (from west to east): (i) the Phulad and Kaliguman shear zones bounding the bulk of the Delhi mobile belt on the west and east, respectively; (ii) the Delwara and Banas Faults that run along the BGC–Aravalli boundary; (iii) the Rakhabdev Fault that splits the Aravalli mobile belt into a platform sequence in the east and a turbidite sequence in the west; and (iv) the Great Boundary Fault running along the eastern boundary of the Aravalli terrain (Fig. 1). Among these lineaments, the Phulad shear zone and Rakhabdev Fault are regarded as the Proterozoic suture zones in the plate tectonic model for the evolution of the Aravalli range (Sinha-Roy *et al.* 1998).

The Great Boundary Fault (GBF), the focus of this study, crops out for > 400 km from Sapotara in the NE to Chittaurgarh and beyond in the SW (Fig. 1). Geophysical surveys have imaged the subsurface extension of the GBF for another 400 km north of Sapotara, under the Gangetic alluvium (Tiwari, 1995). Dipping at a steep angle to the NW, the GBF occurs as reverse fault that emplaces the pre-Vindhyan rocks over the younger platform sediments of the Vindhyan Supergroup (Ray *et al.* 2002). A series of small tear faults punctuate the GBF sporadically.

All along its strike length from Sapotara to Parsoli, the GBF runs parallel to the NNE–NE-trending folds in the adjacent Vindhyan sediments (Figs 2a, b, 3a). However, an exception seems to occur near Chittaurgarh, where the NE-trending GBF apparently truncates the N–S-trending folds in the Vindhyan sediments (Fig. 3b; Sinha-Roy *et al.* 1986). SW of Chittaurgarh, the GBF swerves to assume a parallelism with the N–S-trending folds. The study area around Chittaurgarh is therefore a pivotal point in the geometry of the GBF. With the help of satellite imagery, high-resolution outcrop mapping and structural analysis, we describe the structural characteristics and tectonic setting of the GBF around the Chittaurgarh area.

https://doi.org/10.1017/S0016756821000157 Published online by Cambridge University Press

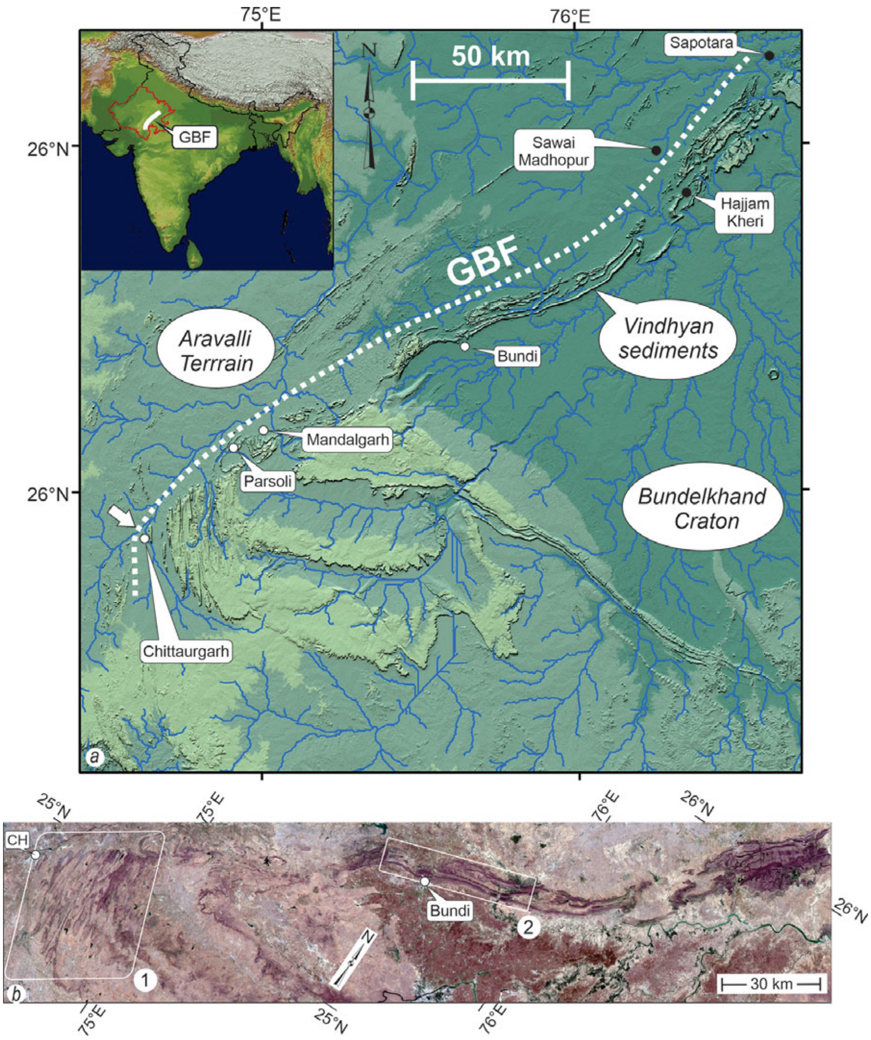

Fig. 2. (Colour online) Tectonic setting of the Great Boundary Fault (GBF). (a) Digital elevation model (DEM). N–S-trending folds appear truncating against the NE-trending GBF between Chittaurgarh and SW of Parsoli in the southwestern part. White arrow points to bend in the GBF around Chittaurgarh, the study area. (b) Anaglyph; DEMs of two areas, enclosed in rectangles 1 and 2, are shown in Figure 3a and b, respectively. CH – Chittaurgarh. Compare with (a) for the GBF trace and other locations. Observations through red–blue or red–cyan glasses provide distinct 3D visualization of the refolding.

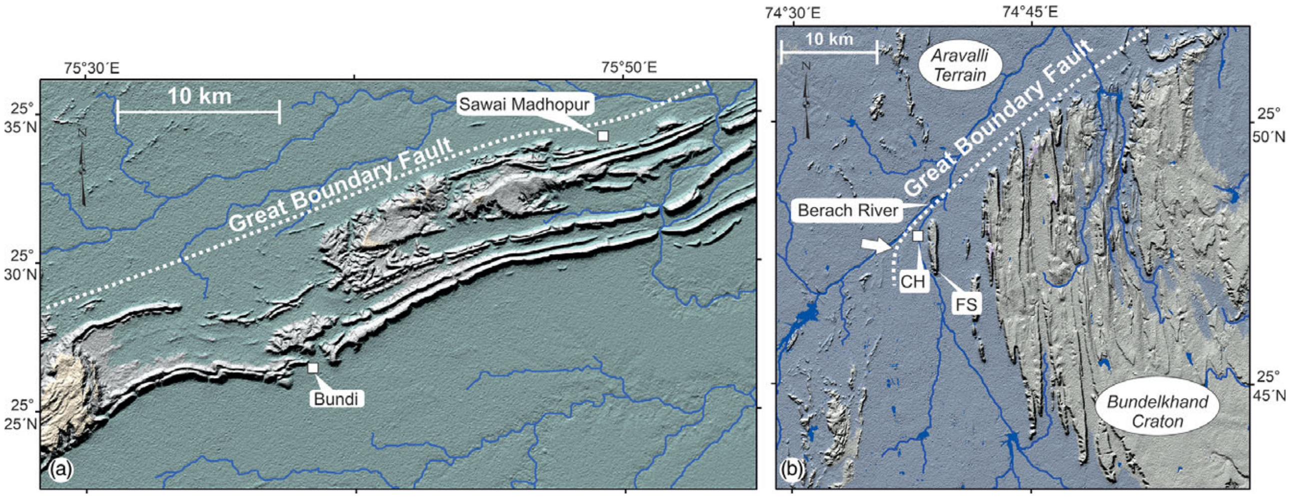

Fig. 3. (Colour online) DEM images of the two areas in rectangles 1 and 2 in Figure 2b. (a) GBF runs parallel to ENE-trending folds in the NE and middle sectors. (b) In the SW sector, NE-trending GBF runs obliquely to N–S-trending folds (e.g. FS). White arrow points to the bend in the GBF around Chittaurgarh. CH – Chittaurgarh; FS – Fort synform.

3. Evidence from satellite imagery

We used two types of remote sensing datasets to decipher the large-scale structural pattern in the GBF: (i) 149 tiles of a digital elevation model (DEM) from the Advanced Land Observing Satellite (ALOS) Phased Array type L-band Synthetic Aperture Radar (PALSAR) data; and (ii) 14 scenes of Sentinel-2 multispectral data in 13 bands with 10, 20 and 60 m spatial resolution and 290 km

https://doi.org/10.1017/S0016756821000157 Published online by Cambridge University Press

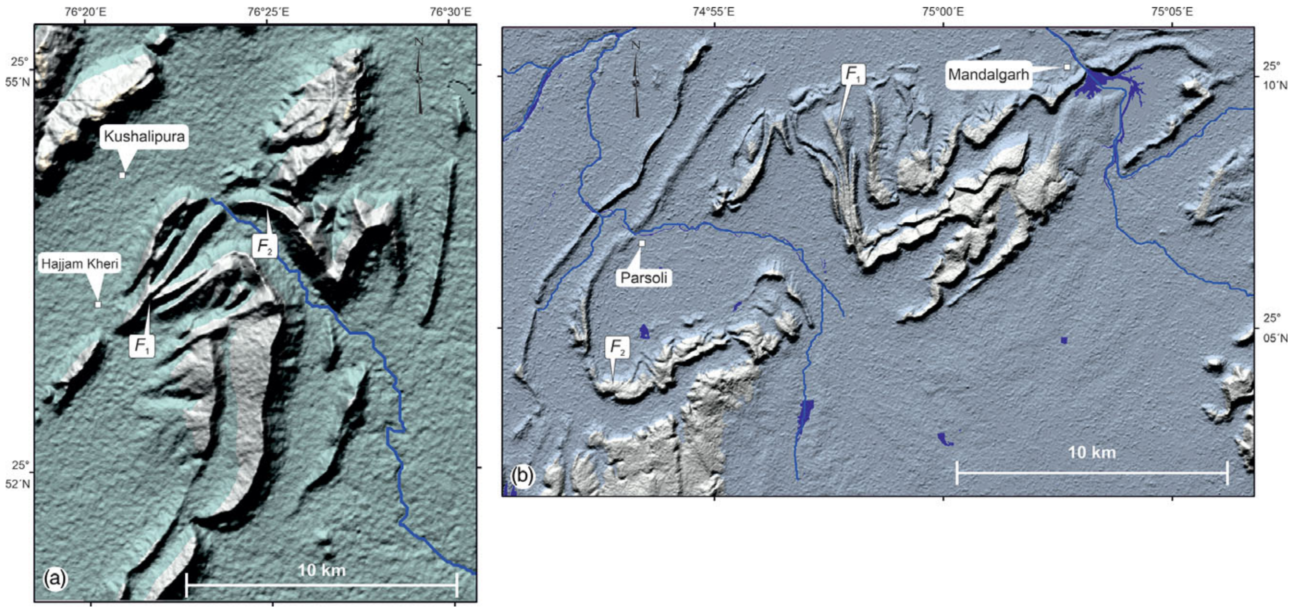

Fig. 4. (Colour online) DEM showing examples of characteristic refolding in the GBF. (a) NE segment of the GBF around the Kushalipura–Hajjam Kheri area. (b) SW segment around the Mandalgarh–Parsoli area. F_1 – early fold; F_2 – late fold.

field of view. A combination of principal component analysis and different filters was used for image enhancement. Superimposition of the geological features, extracted from Sentinel images and the ALOS PALSAR DEM, brought out the characteristic structural pattern in the GBF (Figs 2–4). Observing the anaglyph images obtained from the Sentinel images through red-blue or red-cyan glasses provides three-dimensional (3D) visualization of the structures in the GBF (Fig. 2b). A description of the remote sensing techniques used in this study is provided in online Supplementary Material S1 (available at http://journals.cambridge.org/geo).

LandSat imagery and the DEM reveal that the GBF is a tectonic zone that contains intensely deformed Vindhyan sediments (Fig. 2a, b). The width of this zone varies from 10–15 km to 200–300 m. The processed images show distinct refolding of the early folds by the late folds over the entire GBF. Here, we present two typical examples of large-scale structures in the GBF. The first example is from the NE sector of the GBF around Kushalipura–Hajjam Kheri area (Fig. 4a). The second example shows refolded folds in the SW sector of the Mandalgarh–Parsoli area (Fig. 4b). Both examples highlight the occurrence of refolded folds in the GBF zone.

4. GBF around Chittaurgarh

A simplified stratigraphic order of the lithounits across the GBF is given in Table 2. The Berach Granite, a component of the Banded Gneissic Complex, occupies the low-lying plains in the hanging wall of the GBF. On the GBF footwall, the synclinal hills and anticlinal valleys expose the Kaimur Sandstone – Suket Shale beds and the Nimbahera Limestone–Nimbahera Shale beds, respectively (Fig. 5a).

This study is based on the observations along the Berach River Fort section that exposes the GBF core and the damage zone (Caine *et al.* 1996; Choi *et al.* 2016). We distinguish the core from the damage zone on the basis of characteristic structures and contrast in deformation intensity (Table 2). Three successive phases of folds, F_1, F_2 and F_3, and ductile shear zones are the characteristic structures in the shale beds occupying the core. By contrast, the damage zone rocks, affected by only a single phase of folding, are cut by the mesoscopic-scale brittle-ductile shear zones and striated faults. The deformation intensity, inferred qualitatively from frequency distribution and complexity of structures, is higher in the core than in the damage zone. The damage zone-core boundary runs approximately along the lithological contact between the Nimbahera Limestone and Nimbahera Shale beds (DZ and FC in Fig. 5a). With progressive decrease in the intensity of deformation towards the east, the damage zone grades into undeformed wall rock, the flat-lying Vindhyan sediments.

4.1. The GBF damage zone

The bedding surface (S_0) in the damage zone is deformed into N–S trending and open to gentle large-scale F_1 folds. The Fort synform is a typical example of the large-scale structure in the damage zone (Fig. 5a, b). A weak axial plane cleavage (S_1) is occasionally associated with the F_1 folds, in particular, in the limestone beds (Fig. 6). The mesoscopic-scale structures characterizing the damage zone are the conjugate pairs of brittle-ductile shear zones (BDSZ) containing en échelon veins and striated faults (Fig. 7a–c). Oriented consistently on the limbs and hinge zone, the BDSZ and striated faults post-date the large-scale F_1 folding.

The angular relationship between the en échelon veins and the shear zone boundary reveals unambiguous shear sense in the BDSZ (Ramsay & Huber, 1983). Similarly, the slip direction is inferred along a line that is perpendicular to the intersection of veins and shear zone boundary. These criteria reveal horizontal-dextral and horizontal-sinistral shear sense in the complementary sets of conjugate BDSZ. Without exception, the veins in the sandstone and limestone beds are infilled by quartz and carbonate minerals, respectively. Such a strong lithological control on vein composition implies that the syntectonic fluids were derived from the respective host rocks. A fluid inclusion study by Srivastava & Sahay (2003) reveals the development of the BDSZ by syntectonic Na-Ca-Cl brines at 160–200°C temperature and 53 MPa pressure.

https://doi.org/10.1017/S0016756821000157 Published online by Cambridge University Press

Table 2. Lithounits and structural characteristics in the GBF core and damage zone in the study area. GBF – Great Boundary Fault.

Supergroup/fault	Formation	Structural position	Structural characteristics
Upper Vindhyan Group	Kaimur Sandstone (*c.* 1100 Ma; McKenzie *et al.* 2011)	GBF damage zone	Large-scale single-phase folds (F_1)
Lower Vindhyan Group	Suket Shale, Nimbahera Limestone, Nimbahera Shale	GBF core	Mesoscopic-scale brittle-ductile shear zones, en échelon veins and striated faults; polyphase folds (F_1, F_2 and F_3), deformed lineations and ductile shear zones
Banded Gneissic Complex, GBF	Berach Granite (*c.* 2500 Ma; Wiedenbeck *et al.* 1996)	Hanging wall of the GBF	Mostly undeformed and porphyritic

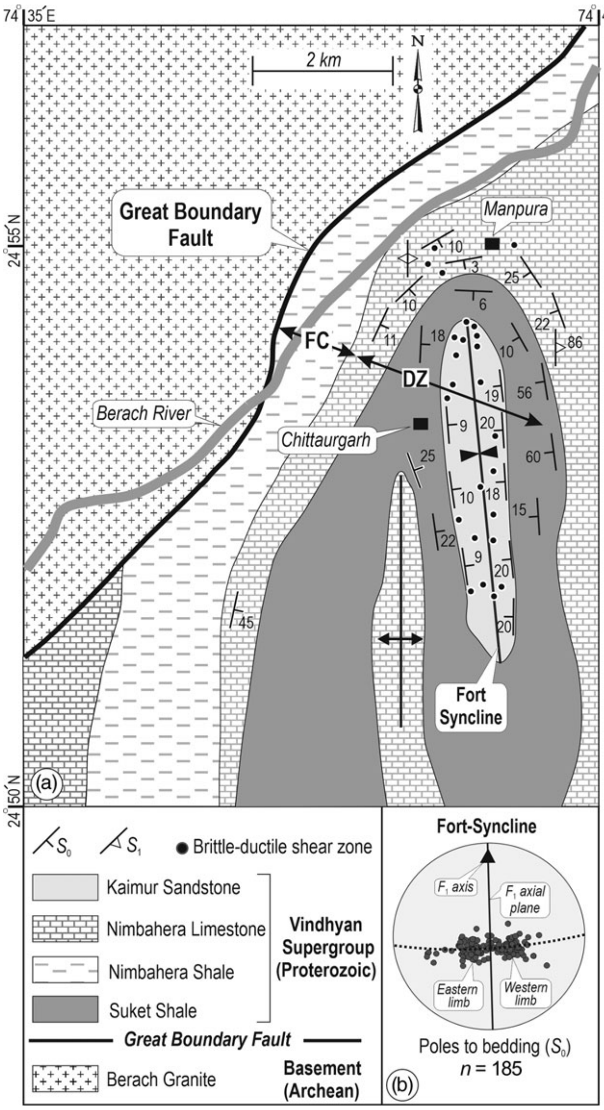

Fig. 5. (a) Geological map of the study area (after Prasad, 1984). FC (core) and DZ (damage zone) of the GBF in the Berach River–Fort section. (b) Lower-hemisphere equal-area projection of poles to bedding surface in a large-scale F_1 fold, the Fort synform, in the damage zone (after Srivastava & Sahay, 2003).

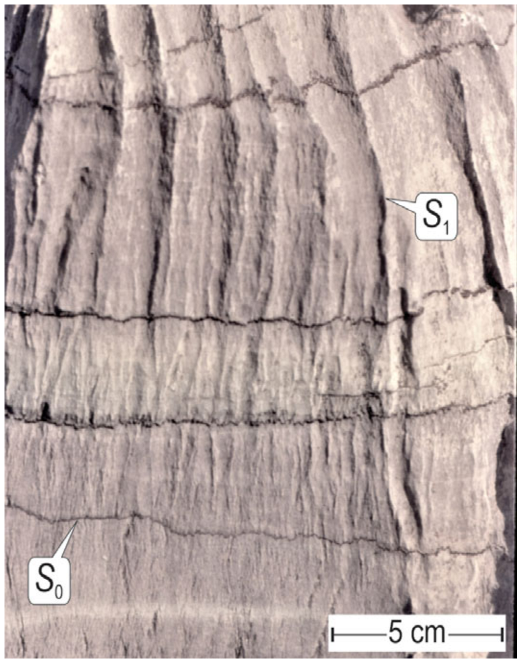

Fig. 6. (Colour online) Sub-horizontal bedding (S_0) and N–S-striking upright axial plane cleavage (S_1) around an F_1 fold hinge zone in the damage zone. Rock type: Nimbahera Limestone.

In addition to the BDSZ, two groups of mesoscopic-scale striated faults cut through the damage zone rocks. The first group consists of conjugate pairs of strike-slip faults that are characterized by sub-vertical dip angles and sub-horizonal striae (Figs 7b, 8a). The orientations, slip sense and slip direction on the striated strike-slip faults and the corresponding BDSZ are consistent. The second group of striated faults contains conjugate pairs of thrusts (Figs 7c, 8b). Striae on the thrusts reveal a dominantly up-dip movement of the hanging wall. We used the direct inversion method for palaeostress estimation from the strike-slip faults and the BDSZ, and the thrusts (Angelier, 1990, 1994; Srivastava *et al.* 1995; Srivastava & Sahay, 2003). The results show that the striated strike-slip faults/brittle-ductile shear zones and the thrusts are compatible with horizontal ENE–WSW-directed maximum compression, σ_1 (Fig. 8a, b). However, the shape factor, $\phi = (\sigma_2{-}\sigma_3)/(\sigma_1{-}\sigma_3)$, determined via palaeostress analyses, is insignificant due to the Andersonian geometry of the BDSZ and the striated faults (Angelier, 1994). In a recent review, Lacombe (2012) addresses the issues related to palaeostress estimation from the inversion of fault-slip data and a comparison with the contemporary stress patterns.

4.2. The GBF core

The GBF core, a zone of intense deformation in the Nimbahera Shale, is spectacularly exposed along the Berach River flowing in

Fig. 7. (Colour online) Characteristic mesoscopic structures in GBF damage zone. (a) Conjugate pair of strike-slip brittle-ductile shear zones containing en échelon quartz veins (plan view; S_0 is sub-horizontal and the veins are upright). Half-barbed arrows indicate shear sense. (b) An upright striated strike-slip fault. The slip direction is horizontal (parallel to striae) and slip-sense is dextral. White arrow – direction of movement of the missing block. (c) A striated thrust cuts the sub-horizontal bedding surface (S_0) at a low angle. Hanging wall moves in the direction of black arrow. All examples are from the sandstone beds on the western limb of the Fort synform.

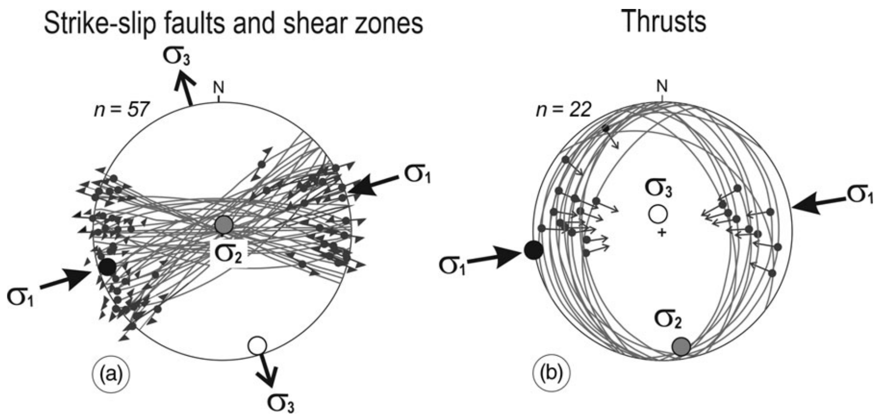

Fig. 8. Results of palaeostress analysis in the damage zone. (a) Strike-slip structures, faults and brittle-ductile shear zones. (b) Compressional structures, thrusts. σ_1 orientation is consistent in (a) and (b). After Srivastava & Sahay (2003).

the vicinity of the Berach Granite. The core is characterized by numerous metre-scale doubly-plunging en échelon folds and thin mylonite-bearing ductile shear zones. Outcrop-scale refolded folds and deformed lineations are common in the core. In contrast to the damage zone, the core lacks any brittle-ductile shear zones, en échelon veins or striated faults. We highlight the deformation style in the GBF core by using the evidence from high-resolution outcrop mapping and structural analysis of the mesoscopic-scale fabric data.

4.2.a. Folds

Overprinting relationships, such as the refolded folds and deformed intersection lineations, help to distinguish three successively developed fold groups (F_1, F_2 and F_3) in the GBF core (Figs 9a, b, 10a, b). F_1 folds, developed on bedding surfaces (S_0) and intrafolial quartz veins, occur as variably oriented isoclines and rootless hinge zones. Deformed intersection lineations (S_0/S_1), occurring as curvilinear traces on F_2 fold surfaces, imply a non-coaxial refolding of F_1 folds during F_2 folding (Fig. 9b).

Characteristically open to close and symmetric to asymmetric F_2 folds, traced by S_0//S_1 surfaces, are ubiquitous in the GBF core. In contrast to the heterogeneously oriented F_1 folds, F_2 folds are characterized by consistently NNE–NE-striking upright axial planes and doubly-plunging hinge lines. Evidence from the outcrop-scale refolded folds reveals that the variation in F_1 fold orientation is primarily due to the superposition of F_2 folds (Fig. 10a). F_1 folds occurring on F_2 hinge zones and limbs are commonly recumbent and reclined, respectively (Fig. 10b). Several outcrops show such an en échelon arrangement of F_2 folds that implies dextral shear sense in the GBF core (Fig. 11). The hinge line bifurcation, an artefact of buckling (Sahay & Srivastava, 2005*a*), is yet another characteristic of F_2 folds in the GBF core. Commonly, an antiform bifurcates into two such branch antiforms that share a common synform. The resultant hourglass outcrop pattern juxtaposes the main antiform and shared synform along a common axial trace (Fig. 12a). F_3 folds, trending characteristically NNW–NW, are infrequently developed as broad warps. Although rare, the interference between F_2 and F_3 produces axial culminations, consisting of curvature accommodation folds, at a few outcrops (Fig. 12b). Both F_2 and F_3 folds lack any axial plane cleavage.

4.2.b. Deformed intersection lineations

F_2 fold surfaces commonly contain deformed intersection lineations that represent curvilinear F_1 hinge lines (Fig. 9b). We traced these lineations by overlaying transparent sheets on individual F_2 folds. Upon unrolling the tracings about F_2 hinge lines, the F_1 lineations assumed a dominantly ENE–WSW-directed rectilinear pattern (Fig. 13a, b). Two inferences can be drawn from such unrolled patterns: (i) F_1 hinge lines were dominantly trending ENE–WSW before the superimposition of F_2 folds; and (ii) F_2 folds were developed by the flexural-slip mechanism (Ramsay, 1967; Ghosh & Chatterjee, 1985; Ramsay & Huber, 1987). Several other lines of evidence supporting flexural-slip during F_2 folding are class 1B fold geometry and the occurrence of hinge-line-normal striae on the bedding surfaces.

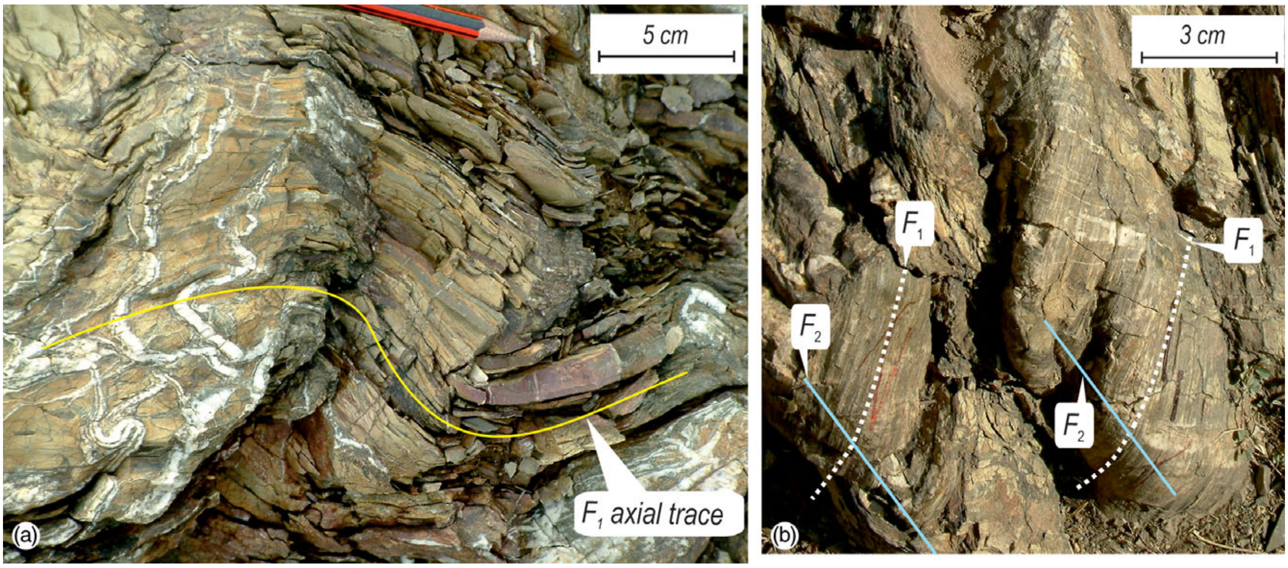

Fig. 9. (Colour online) Overprinting relationships in the GBF core. (a) Open and asymmetric F_2 folds refold the F_1 folds traced by thin quartz veins. F_1 axial trace, marked by yellow line, is parallel to S_1. (b) Traces of thin quartz veins occur as deformed F_1 lineations on F_2 fold surfaces. Rock type: Nimbahera Shale.

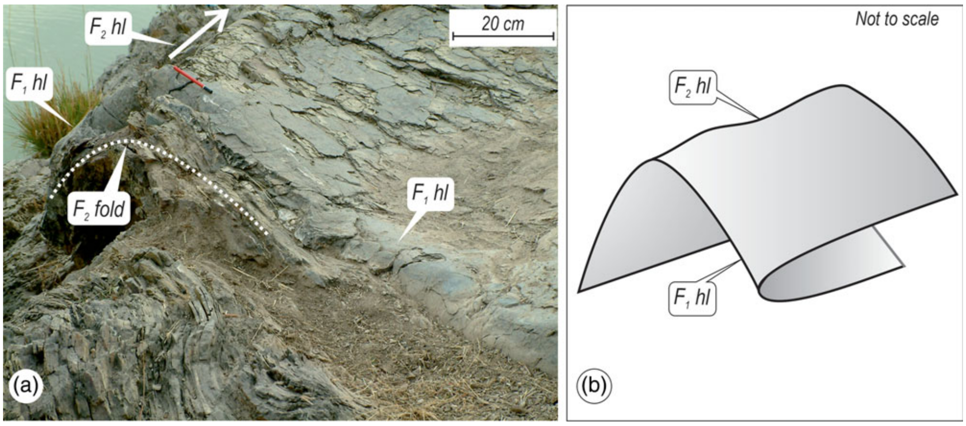

Fig. 10. (Colour online) Relationship between F_1 and F_2 folds in the GBF core. (a) Refolding of an isoclinal F_1 fold by an upright-non-plunging F_2 fold trending 042°. F_1 hinge line plunges at variable angles. (b) Schematic diagram shows refolding of an F_1 fold by F_2 fold. F_1 fold geometry varies from recumbent to reclined on the hinge zone and limbs of F_2 fold, respectively. hl – hinge line. Rock type: Nimbahera Shale.

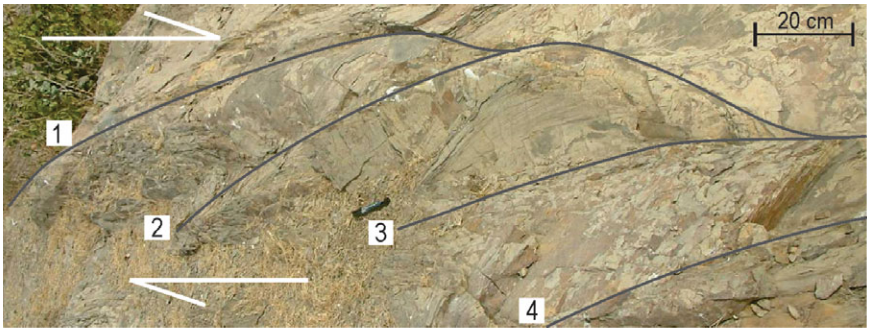

Fig. 11. (Colour online) En échelon arrangement of doubly-plunging F_2 folds suggests dextral shear sense in the GBF core. Rock type: Nimbahera Shale. 1–4 – hinge lines.

4.2.c. Shear zones

Numerous decimetre-thin ductile shear zones occur as characteristic structures in the GBF core (Sahay & Srivastava, 2005*b*). Typically, the shear zones consist of mylonitized quartz veins, millimetre-thin dark phyllonite bands and oxidized opaques. Based on the angular relationship with the bedding surface, we classify the shear zones into three descriptive types: (i) concordant shear zones that run parallel to bedding surface and trace F_2 folds (Fig. 14a, b); (ii) discordant shear zones that cut across F_2 folds (Fig. 14c); and (iii) hybrid shear zones that are partly concordant and partly discordant. Two sets of quartz veins, V_1 and V_2, are associated with the shear zones. V_1 veins run parallel to the bedding surfaces (S_0) tracing the isoclinal F_1 folds. V_2 veins cut across the V_1 veins and show characteristic lateral offsets along the shear

https://doi.org/10.1017/S0016756821000157 Published online by Cambridge University Press

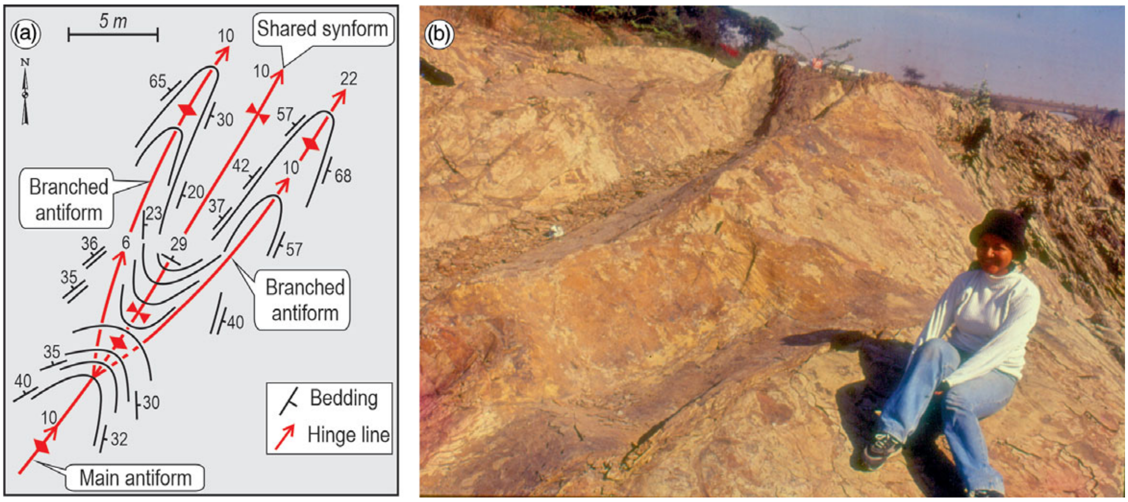

Fig. 12. (Colour online) Hourglass map pattern and culmination in the GBF core. (a) Bifurcation of a fold hinge line juxtaposes the main antiform and shared synform along a common axial trace, and produces an hourglass map pattern. After Sahay & Srivastava (2005*a*). (b) Axial culmination in subarea IV. Student Priyanka Hazarika for scale. Rock type: Nimbahera Shale beds.

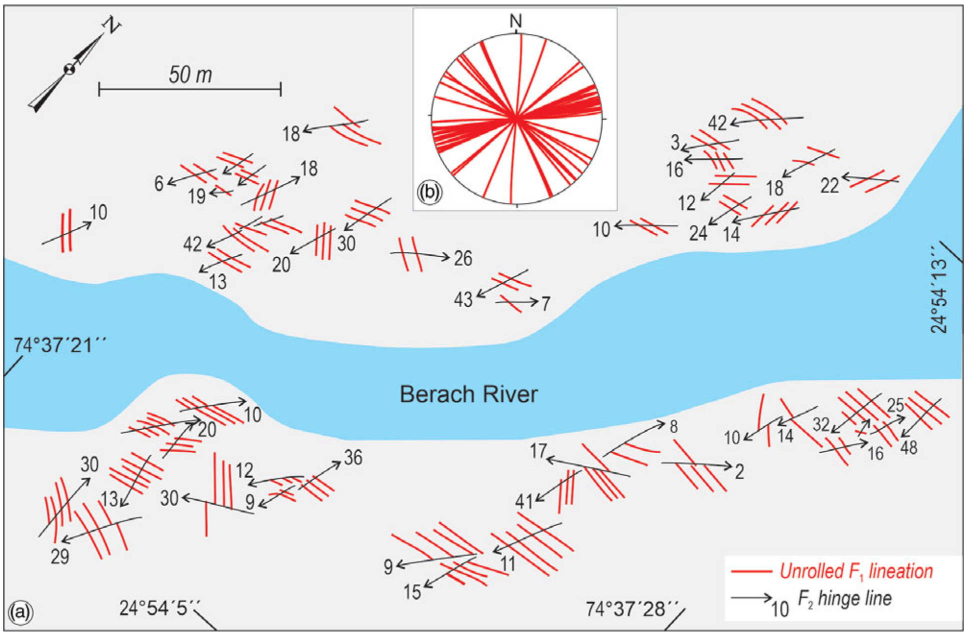

Fig. 13. (Colour online) (a) Unrolled patterns of deformed intersection lineations (F_1) occurring in F_2 folds in the Nimbahera Shale beds. (b) Rosette obtained by scaling and overlapping mid-points of 49 unrolled F_1 lineation patterns. ENE–WSW-directed rectilinear patterns are predominant.

surfaces (Fig. 14b). The ductile shearing initiated during or before F_2 folding and outlasted the development of F_2 folds and V_2 veins in the GBF core.

Microstructures, such as the *S-C* (*schistosité et cisaillement*) fabric, dominos and asymmetric quartz boudins are common in all three types of shear zones (Fig. 14b, c). Different stages of dynamic recrystallization can be traced through microstructures in the shear zones. The core-and-mantle structure, containing σ-porphyroclasts, represents an early stage of mylonitization (Fig. 15a). With a progressive increase in the intensity of shearing, the mylonite assumed a banded structure that consists of alternate bands of coarse quartz-ribbons and biotite-rich fine-grained recrystallized quartz (i and ii in Fig. 15b). Finally, the static recrystallization took over the dynamic recrystallization, resulting in development of foam texture (Fig. 15c; Hobbs *et al.* 1976; Passchier & Trouw, 1998).

5. Structural characteristics of the GBF core

The structures on both banks of the Berach River, exposing the GBF core, are similar. For the sake of brevity, we therefore present the structural analysis of the GBF core exposed on the NW bank. Based on the homogeneity in F_2 hinge line orientation, we divided the GBF core into four subareas, I to IV (Fig. 16). In each subarea, high-resolution mapping by the tape-and-compass method was followed by structural analysis by routine techniques (Turner & Weiss, 1963; Ramsay, 1967; Ramsay & Huber, 1987). The mapping scale varies from 1:400 to 1:100 depending upon the complexity of structures in the individual subareas. F_1 folds are too small and F_3 folds are too rare for map representation; our maps therefore show the distribution of F_2 folds and ductile shear zones (Figs 17–19). The rock type in all four subareas is Nimbahera Shale.

https://doi.org/10.1017/S0016756821000157 Published online by Cambridge University Press

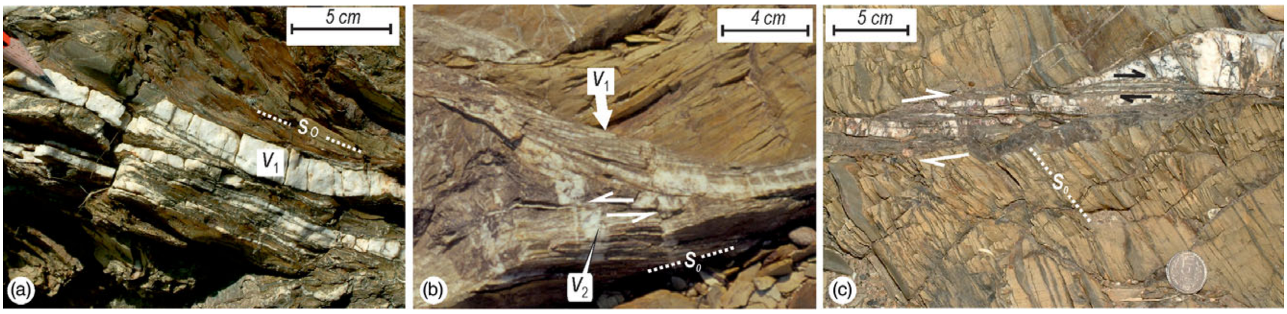

Fig. 14. (Colour online) Ductile shear zones in the Nimbahera shale beds of the GBF core. (a) A concordant shear zone running parallel to bedding (S_0). V_1 quartz veins run parallel to the mylonite foliation in the shear zone. (b) Thin V_1 veins trace isoclinal F_1 fold (indicated by thick white arrow) in a concordant shear zone (after Sahay & Srivastava, 2005*b*). Thick V_2 veins, cutting across the V_1 veins, are offset sinistrally. (c) Discordant shear zone contains a domino structure that is made up of imbricated quartz veins. S_0 – bedding surface.

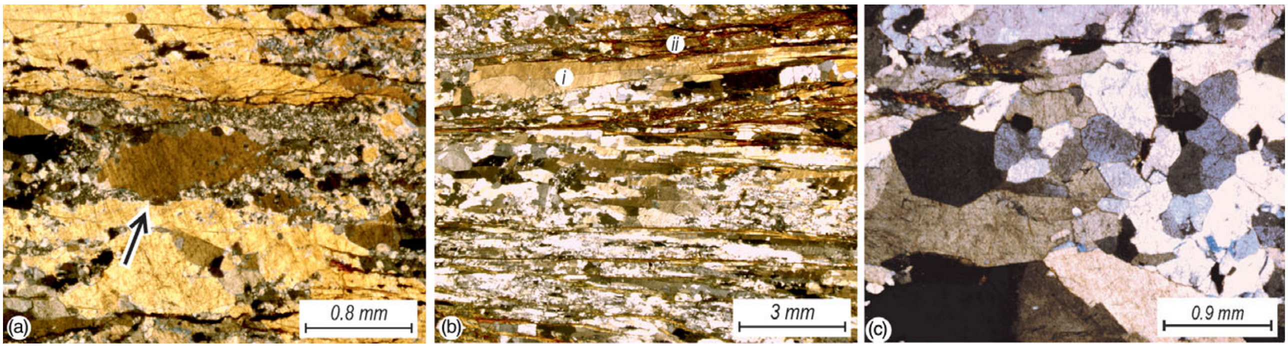

Fig. 15. (Colour online) Microstructures in shear zone mylonites in the GBF core (cross-polarized light). (a) Core-and-mantle structure produced as a result of subgrain rotation during dynamic recrystallization. Arrow indicates a σ-porphyroclast. (b) Mylonite containing alternate bands of ribbon-quartz (i) and biotite-rich fine-grained quartz (ii). (c) Foam texture formed as a result of static recrystallization. (a) and (b) after Sahay & Srivastava (2005*b*).

5.a. Structural analysis

Among the three groups of folds in the GBF core, NNE–NE-trending and doubly-plunging F_2 folds are abundant in all subareas (Figs 17–19). Branched fold hinge lines, sigmoidal axial traces and hourglass structures are the common outcrop patterns in the GBF core. The starfish-like outcrop pattern in subarea IV represents an axial culmination that contains several curvature-accommodation folds (Fig. 19a; Lisle *et al.* 1990). Table 3 summarizes the results of structural analysis in individual subareas I–IV.

5.b. Generalized structural pattern

The generalized structural architecture of the GBF core is obtained by synoptic analysis that combines the observations from all four subareas (Fig. 20a–g). Both the synoptic structural analysis and the map patterns reveal that the F_2 folds control the structural geometry of the GBF core. Over the large scale, the bedding-parallel cleavage surface is folded about the SW-plunging axis that parallels the mesoscopic-scale F_2 fold hinge lines (Fig. 20b, c). F_1 folds, although rarely preserved, are heterogeneously oriented (Fig. 20a). F_3 folds occur as gentle, upright warps that plunge at low to moderate angles towards the NW (Fig. 20e).

The concordant shear zones trace F_2 folds that dominantly plunge at low angles towards the SW (cf. Fig. 20b, f). Stretching lineations on these shear zones are parallel or sub-parallel to F_2 hinge lines in the GBF core (Fig. 20c, f). By contrast, discordant shear zones and corresponding stretching lineations show heterogeneous orientations (Fig. 20g).

Ductile shear zones in the core differ from BDSZ in the damage zone in several respects. First, the BDSZ are consistently oriented, whereas the ductile shear zones are folded and heterogeneously oriented (cf. Figs 8a, 20f, g). Second, the ductile shear zones record a protracted history of shearing from pre- or syn-F_2 to post-F_2 folding, while the BDSZ post-date F_1 folding. Third, the microstructures in the ductile shear zones, such as the bulging recrystallization, subgrain rotation and quartz ribbons (Fig. 15a, b), suggest a peak temperature (> 300°C) that is substantially higher than that for the development of the BDSZ (160–200°C) as determined from a fluid-inclusion study (Srivastava & Sahay, 2003). Finally, the quartz veins in ductile shear zones are commonly mylonitized, whereas those in BDSZ are fibrous and show no recrystallization or cataclastic grain size reduction.

6. Discussion

The polyphase folds are characteristically confined within the GBF core. The damage zone contains single-phase folds that die out into flat-lying sediments towards the east in the interior of the Vindhyan basin. The confinement of folds in the GBF and their progressive disappearance towards the interior of the Vindhyan basin indicate the existence of a genetic link between the folds and the GBF. Whether the polyphase folds in the core formed in three temporally discrete deformation phases or due to flow perturbations during a progressive shearing (Platt, 1983; Hudleston *et al.* 1988; Alsop & Holdsworth, 2002) remains unresolved due to a lack of geochronological data.

https://doi.org/10.1017/S0016756821000157 Published online by Cambridge University Press

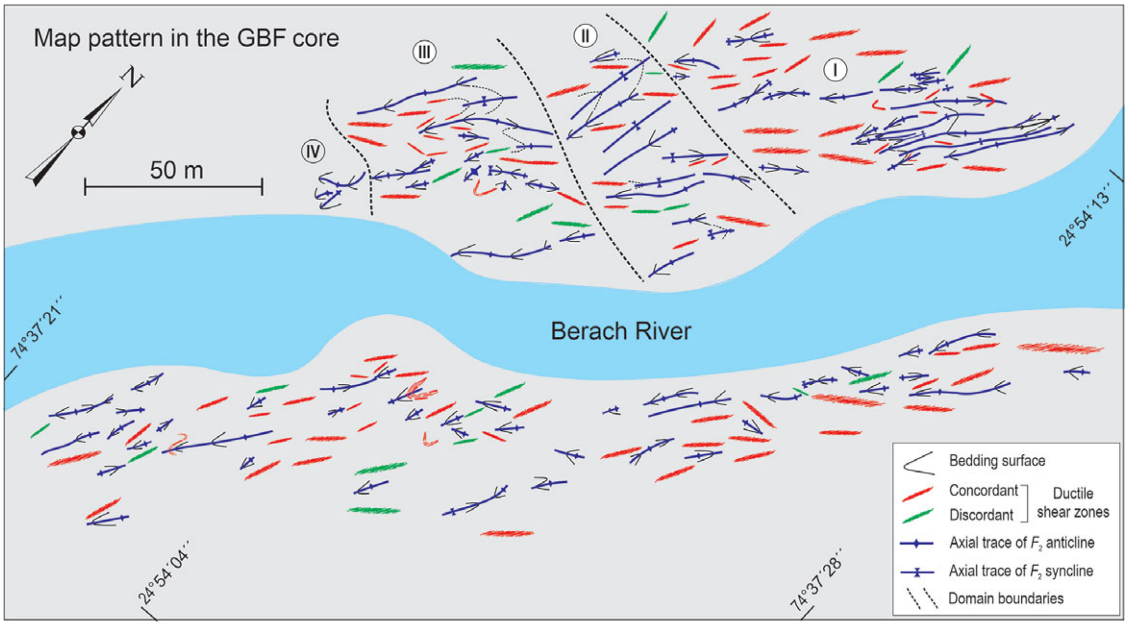

Fig. 16. (Colour online) Fold axial traces and shear zones in the GBF core. Rock type: Nimbahera Shale. Dotted lines mark boundaries of subareas I to IV on the NW bank of Berach River.

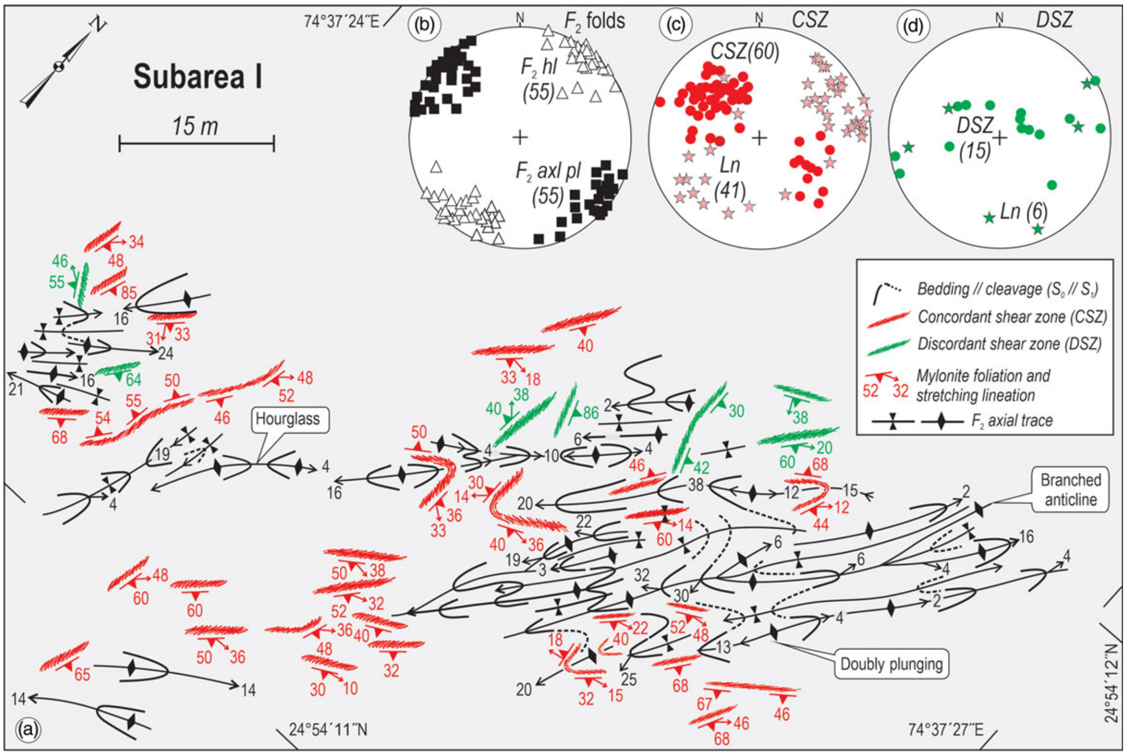

Fig. 17. (Colour online) (a) F_2 folds and shear zones in the shale beds in subarea I of the GBF core (after Sahay & Srivastava, 2005*b*). Concordant shear zones (CSZs) run parallel to bedding surface, whereas discordant shear zones (DSZs) cut across the bedding surface. Gently non-planar doubly-plunging F_2 folds, branched hinge lines and hourglass structures are common. (b) Poles to F_2 axial planes and hinge lines. (c, d) Poles to concordant and discordant shear zones and respective stretching lineations. hl – hinge line; axl pl – axial plane; ln – stretching lineation.

As mentioned in Section 4.1, numerous strike-slip BDSZ faults and thrusts cut through the GBF damage zone. Srivastava & Sahay (2003) propose that the BDSZ and the thrusts correspond to two discrete phases of movements on the GBF. Detailed scrutiny of the outcrops reveals a lack of consistent and unambiguous overprinting relationships between the strike-slip structures and the thrusts. We therefore infer that the strike-slip structures and the thrusts were developed in a common transpressive deformation. This inference is corroborated by the palaeostress directions given by the inversion of fault-slip data (Fig. 8a, b). Both the strike-slip structures and thrusts are compatible with the horizontal ENE–WSW-directed maximum compression σ_1 (Fig. 8a, b). It is likely that an episodic interchange

https://doi.org/10.1017/S0016756821000157 Published online by Cambridge University Press

Table 3. Outline of structural characteristics in subareas I to IV in the GBF core (Fig. 16). CSZ – concordant shear zone; DSZ – discordant shear zone; Ln – stretching lineations.

Subarea	Map pattern	Ductile shear zones
I	NE-trending and low-plunging F_2 folds control map pattern (Fig. 17a, b). Doubly-plunging branched folds and hourglass patterns are common	CSZ trace F_2 folds; Ln on *CSZ* sub-parallel F_2 hinge lines (Fig. 17c); inconsistently orientated DSZ (Fig. 17d)
II	Predominantly SW-plunging F_2 folds trend NNE and NE in western and eastern parts, respectively (Fig. 18a, i)	As for subarea I (Fig. 18a, ii and iii)
III	Doubly-plunging, non-planar and branched F_2 folds (Fig. 18b). Mild axial culminations-depressions and sigmoidal axial traces are common (Fig. 18b, iv)	CSZ and DSZ are common in western and eastern parts, respectively (Fig. 18b); Ln on CSZ sub-parallel F_2 hinge lines (Fig. 19b, iv and v); DSZ are inconsistently oriented (Fig. 18b, vi)
IV	Starfish-like outcrop pattern occurs due to axial culmination containing curvature-accommodation folds (Fig. 19a); scattered orientations of F_2 folds (Fig. 19b)	Absent

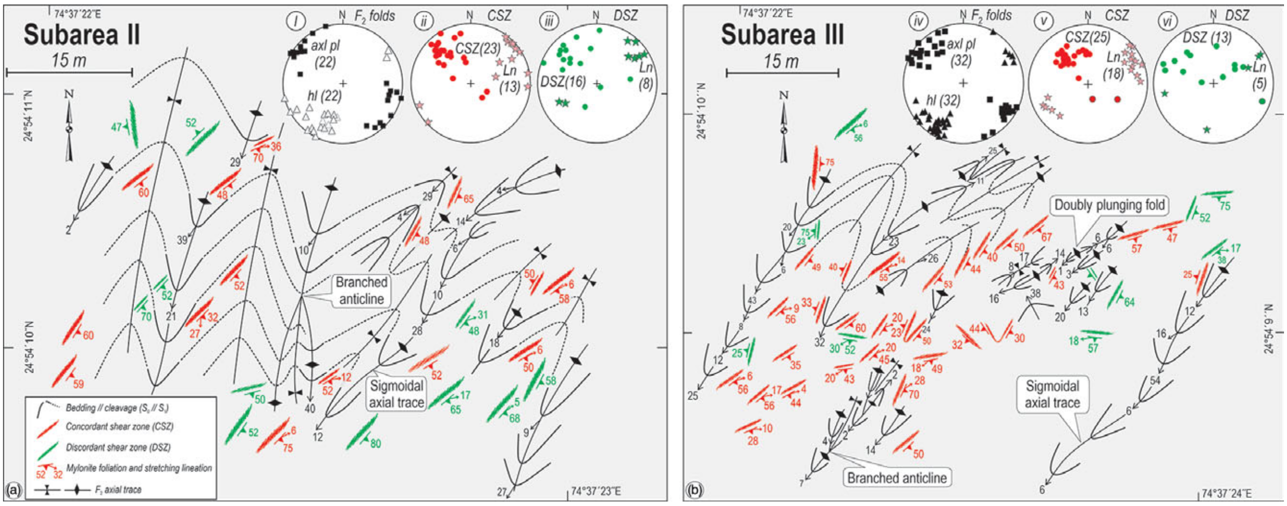

Fig. 18. (Colour online) (a) F_2 folds and shear zones in the shale beds in subarea II of the GBF core. NNE-trending F_2 folds assume NE trend in the eastern part due to increased shearing intensity. (b) Subarea III: sigmoidal, doubly-plunging and branched folds are common in the eastern part. (i–vi) Lower-hemisphere equal-area projections. hl – hinge line; axl pl – axial plane; ln – stretching lineation.

in the local stresses, σ_2 and σ_3, in a regionally transpressive regime resulted in the development of strike-slip structures and thrusts in the damage zone.

The orthorhombic symmetry of conjugate structures, namely the BDSZ, strike-slip faults and thrusts, and the symmetric geometry of large-scale folds (e.g. the Fort synform), point to a contraction or pure-shear-dominated deformation in the damage zone. By contrast, several lines of evidence, such as the en échelon fold arrangement (Fig. 11), rotated *S*-surfaces in ductile shear zones (Fig. 14b), imbricate quartz veins in dominos (Fig. 14c), rotated σ-porphyroclasts (Fig. 15a) and asymmetric boudins all indicate a wrench or simple shear-dominated deformation in the GBF core.

Two main lines of evidence reveal dextral shear sense in the transpression. First, the en échelon pattern of F_2 folds is consistent with dextral shear sense (Fig. 11). Second, ENE–WSW-directed horizontal σ_1, obtained from palaeostress analysis of striated faults, the BDSZ and thrusts (Fig. 8a, b), is consistent with dextral shear sense on the NE-striking GBF around Chittaurgarh. Combining the above lines of evidence, we interpret a strain-partitioned dextral transpression in the GBF in the study area (Fig. 21). The contrast in lithology and mechanical anisotropy, with respect to the compositional layering, fissility and ease of inter-layer slip, may have contributed to strain partitioning in the GBF.

According to Sinha-Roy (2007), an oblique convergence led to the impingement of the dominantly granitic and rigid Bundelkhand craton on the Aravalli terrain during the Neoproterozoic period. The indentation resulted in the development of a top-to-the-E piggy-back sequence of reverse faults that includes the GBF as a frontal fault. We note that the GBF runs parallel to the irregular boundary of the rigid indenter, the Bundelkhand craton. Mimicking the bend in the western margin of the Bundelkhand craton, the GBF swerves from NE to N–S near Chittaurgarh. Beyond Sapotara, the northern extension of the GBF diverts from NE to E–W under the Gangetic Alluvium. This diversion in the GBF is also parallel to the Faizabad ridge, a part of the Bundelkhand craton (Tiwari, 1995; Valdiya, 1998). Based on the above observations, we infer that the shape of the Bundelkhand craton controls the curviplanar geometry of the GBF.

7. Conclusions

High-resolution outcrop mapping highlights the structural contrast between the damage zone and core and reveals the relationship between the GBF and the folds. Whereas the map pattern in the GBF core is controlled by NE-trending F_2 folds, the damage zone map pattern is controlled by N–S-trending F_1 folds. Apart from the large-scale F_1 folds, the mesoscopic-scale brittle-ductile

https://doi.org/10.1017/S0016756821000157 Published online by Cambridge University Press

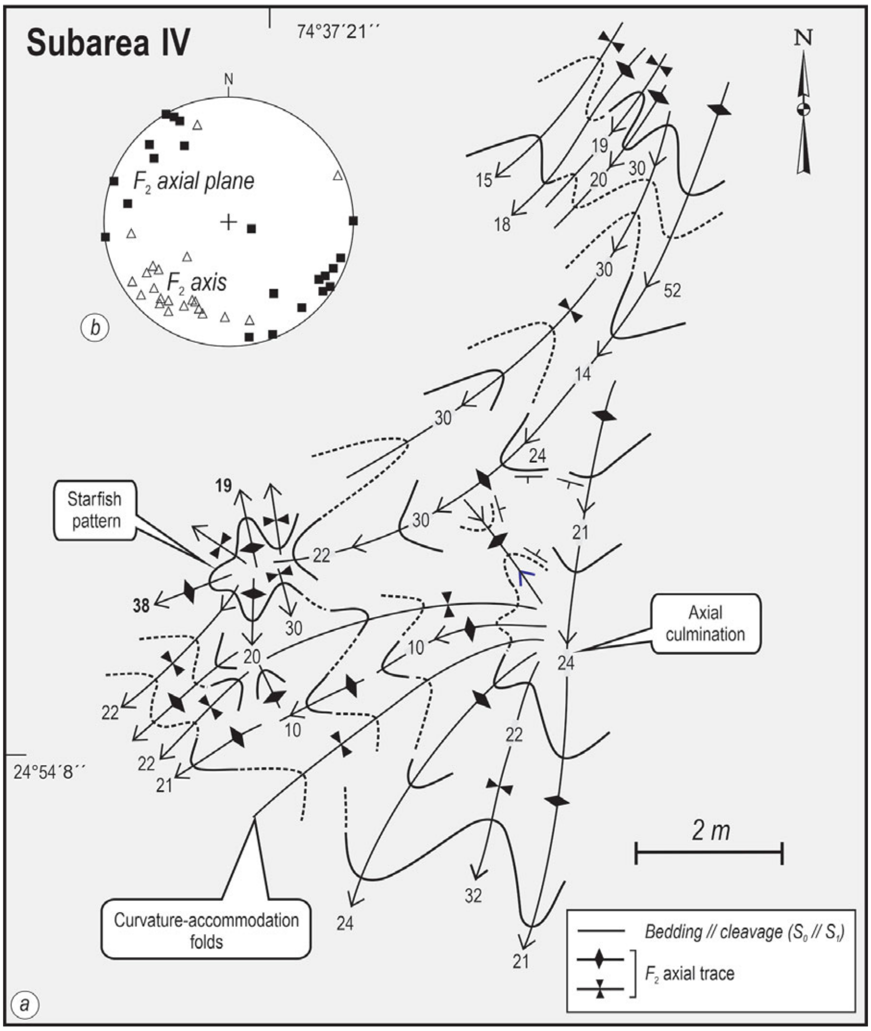

Fig. 19. (a) Map pattern in the shale beds in subarea IV. Starfish outcrop pattern, the axial culmination, contains curvature accommodation folds. (b) Scatter in the F_2 hinge line and axial plane orientations are due to F_3 folding. Lower-hemisphere equal-area projections.

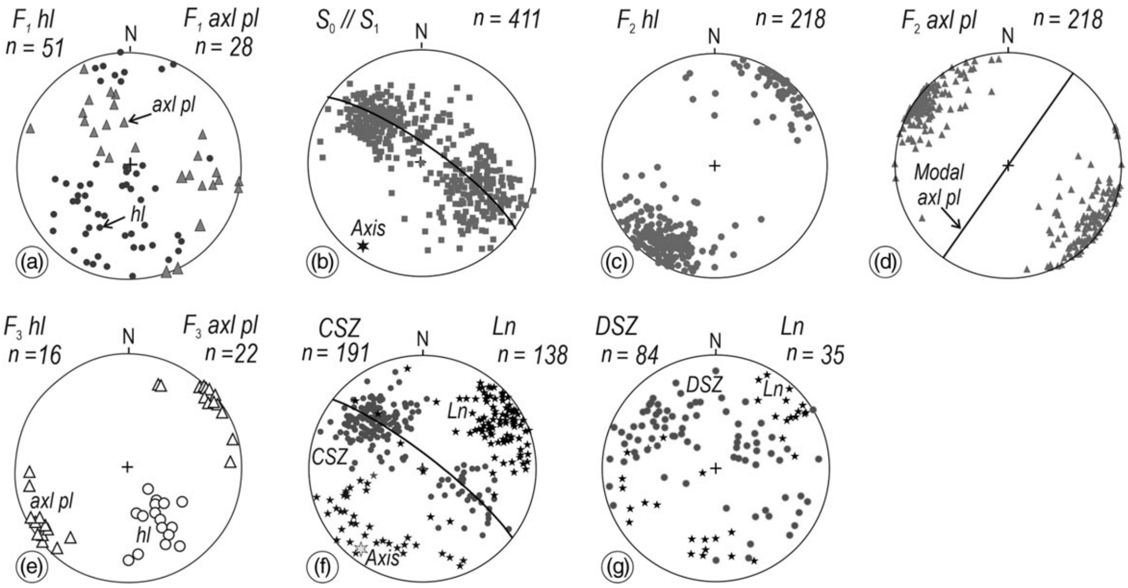

Fig. 20. (a–g) Results of synoptic structural analysis in the GBF core. Lower-hemisphere equal-area projections. S_0 – bedding surface; S_1–F_1 – axial plane cleavage; hl – hinge line; axl pl – axial plane; CSZ – concordant shear zone; DSZ – discordant shear zone; *n* – number of observations.

https://doi.org/10.1017/S0016756821000157 Published online by Cambridge University Press

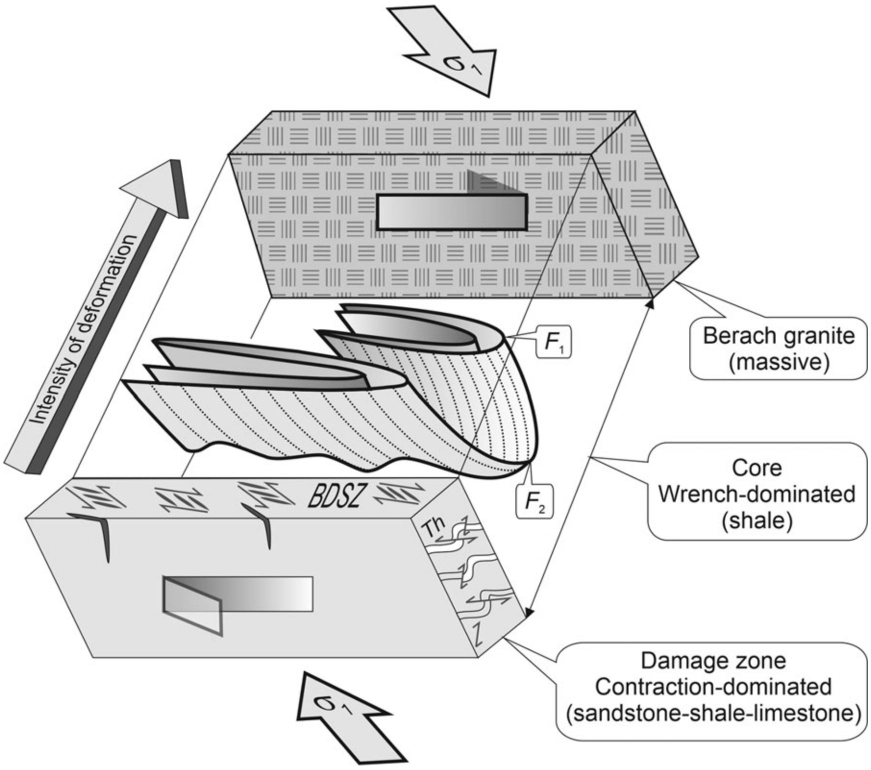

Fig. 21. Schematic model shows prominent representative structures in the strain-partitioned GBF (not to scale). Dotted lines on F_2 fold surfaces represent deformed F_1 lineations. For simplicity, locally developed F_3 folds are not shown. The increase in the intensity of deformation is inferred qualitatively from the frequency distribution and complexity of structures. BDSZ – strike-slip type of conjugate brittle-ductile shear zones containing en échelon veins; Th – conjugate thrusts.

shear zones, en échelon veins and striated faults are the distinctive structures in the damage zone. By contrast, three successively developed fold groups, F_1, F_2 and F_3, and the ductile shear zones are the characteristic structures in the GBF core. Outcrop mapping brings out the parallelism between the GBF and F_2 fold axial traces. Although not evident on the satellite imagery due to the limitation of the scale, F_2 folds are traceable by high-resolution outcrop mapping in the GBF core around Chittaurgarh (Figs 17–19). For several hundred kilometres along its strike length, the GBF runs parallel to F_2 axial traces.

It is well known that the GBF is a reverse fault (Heron, 1936; Coulson, 1967; Iqbaluddin *et al.* 1978; Sinha-Roy *et al.* 1998). However, our study shows that the ENE–WSW-directed oblique compression was partitioned into a dominant contraction in the damage zone and a dominant dextral shearing in the core (Fig. 21). The GBF is a strained-partitioned zone of dextral transpression in the study area.

Acknowledgements. Erudite comments and constructive suggestions from Professor Olivier Lacombe and the two anonymous reviewers helped to improve the manuscript considerably. We are grateful to Gargi Sen, Priya Pachauri and several Masters students for their help during the fieldwork. We thank Elsevier, Current Science and Geological Society of India for permission to reproduce some of the figures from our articles published earlier. This study is funded by JC Bose Fellowship SR-S2-/JCB-46/2012 of the Department of Science and Technology and grant no. 24(0364)/20/EMR-II of the Council of Scientific and Industrial Research, Government of India.

Conflict of interest. None.

References

Allen MB, Alsop GI and Gemchuzhnikov VG (2001) Dome and basin refolding and transpressive inversion along the Karatau Fault System southern Kazakhstan. *Journal of the Geological Society, London* **158**, 83–95.

Alsop GI and Holdsworth RE (2002) The geometry and kinematics of flow perturbation folds. *Tectonophysics* **350**, 99–125.

Angelier J (1990) Inversion of field data in fault tectonics to obtain the regional stress, III. A new rapid direct inversion method by analytical means. *Geophysical Journal International* **103**, 363–76.

Angelier J (1994) Fault slip analysis and paleostress reconstruction. In *Continental Deformation* (ed. PL Hancock), pp. 53–100. Oxford: Pergamon Press.

Caine JS, Evans JP and Forster CB (1996) Fault-zone architecture and permeability structure. *Geology* **24**, 1025–28.

Carreras J, Cosgrove J and Druguet E (2013) Strain partitioning in banded and/or anisotropic rocks: Implications for inferring tectonic regimes. *Journal of Structural Geology* **50**, 7–21.

Choi J, Edwards P, Ko K and Kim Y (2016) Definition and classification of fault damage zones: a review and a new methodological approach. *Earth-Science Reviews* **152**, 70–87.

Choudhuri AK, Gopalan K and Sastry CA (1984) Present status of the geochronology of the Precambrian rocks of Rajasthan. *Tectonophysics* **105**, 131–40.

Choudhuri AR and Guha DB (2004) Evolution of the great boundary fault: a re-evaluation. *Journal of the Geological Society of India* **64**, 21–31.

Coulson MS (1967) The geology of Bundi state, Rajputana. *Records of the Geological Survey of India* **60**, 164–204.

Cruciani G, Montomoli C, Carosi R, Franceschelli M and Puxeddu M (2015) Continental collision from two perspectives: a review of Variscan metamorphism and deformation in northern Sardinia. *Periodico di Mineralogia* **84**, 657–99.

Deb M, Thorpe RI, Krstic D, Crofu F and Davis DW (2001) Zircon U–Pb and galena Pb isotope evidence for an approximate 1.0 Ga terrane constituting the western margin of the Aravalli–Delhi orogenic belt, northwestern India. *Precambrian Research* **108**, 195–213.

Dewey JFE, Holdsworth RE and Strachan RA (1998) Transpression and transtension zones. In *Continental Transpressional and Transtensional Tectonics* (eds RE Holdsworth, RA Strachan and JE Dewey), pp. 1–14. Geological Society of London, Special Publication no. 135.

Dwivedi D, Chamoli A and Pandey AK (2019) Crustal structure and lateral variations in Moho beneath the Delhi fold belt, NW India: insight from

https://doi.org/10.1017/S0016756821000157 Published online by Cambridge University Press

gravity data modeling and inversion. *Physics of the Earth and Planetary Interiors* **297**, 106317.

Fossen H (2016) *Structural Geology* (2nd ed). Cambridge: Cambridge University Press, 524 pp.

Fossen H and Tikoff TB (1993) The deformation matrix for simultaneous simple shearing pure shearing and volume change, and its application to transpression-transtension tectonic setting. *Journal of Structural Geology* **15**, 413–22.

Fossen H and Tikoff TB (1998) Extended models of transpression and transtension, and application to tectonic setting. In *Continental Transpressional and Transtensional Tectonics* (eds RE Holdsworth, RA Strachanand and JE Dewey), pp. 15–33. Geological Society of London, Special Publication no. 135.

Fossen H, Tikoff TB and Teyssier CT (1994) Strain modelling of transpressional and transtensional deformation. *Norsk Geologisk Tidsskrift* **74**, 134–45.

Ghosh S (2001) Types of transpressional and transtensional deformation. In *Tectonic Modelling: A Volume in Honour of Hans Ramberg* (eds HA Koyi and NS Mancktelow), pp. 1–20. Boulder: Geological Society of America, Memoir no. 193.

Ghosh S and Chatterjee A (1985) Patterns of deformed early lineations over later folds formed by buckling and flattening. *Journal of Structural Geology* **7**, 651–66.

Gopalan K, MacDougall JD, Roy AB and Murali AV (1990) Sm-Nd evidence for 3.3 Ga old rocks in Rajasthan, northwestern India. *Precambrian Research* **48**, 287–97.

Graziani R, Montomoli C, Iaccarino S, Menegon L, Nania L and Carosi R (2020) Structural setting of a transpressive shear zone: insights from geological mapping, quartz petrofabric and kinematic vorticity analysis in NE Sardinia (Italy). *Geological Magazine* **157**, 1898–916.

Harland WB (1971) Tectonic transpression in Caledonian Spitsbergen. *Geological Magazine* **108**, 27–47.

Heron AM (1936) Geology of southeastern Mewar, Rajputana. *Memoir of the Geological Survey of India* **68**, 130.

Hobbs BE, Means WD and Williams PF (1976) *An Outline of Structural Geology*. New York: John Wiley and Sons, 571 pp.

Hudleston PJ, Schultz-Ela D and Southwick DL (1988) Transpression in an Archean greenstone belt, northern Minnesota. *Canadian Journal of Earth Sciences* **25**, 1060–68.

Iacopini D, Carosi R, Montomoli C and Passchier CW (2008) Strain analysis and vorticity of flow in the Northern Sardinian Variscan Belt: recognition of a partitioned oblique deformation event. *Tectonophysics* **446**, 77–96.

Iqbaluddin PB, Sharma SB, Mathur RK, Gupta SN and Sahai TN (1978) Genesis of the Great Boundary Fault of Rajasthan, India. In *Proceedings of the Third Regional Conference on Geology and Mineral Resources of Southeast Asia*, Bangkok, Thailand, 14–18 November 1978, pp. 145–49.

Jones RR, Holdsworth RE, Clegg P, McCaffery K and Tavarnelli E (2004) Inclined transpression. *Journal of Structural Geology* **26**, 1531–48.

Jones RR and Tanner PWG (1995) Strain partitioning in transpression zones. *Journal of Structural Geology* **6**, 793–802.

Lacombe O (2012) Do fault slip data inversions actually yield "paleostresses" that can be compared with contemporary stresses? A critical discussion. *Comptes Rendus Geoscience* **344**, 159–73.

Li P, Sun M, Rosenbaum G, Cai K, Chen M and He Y (2016) Transpressional deformation, strain partitioning and fold superimposition in the southern Chinese Altai, Central Asian Orogenic Belt. *Journal of Structural Geology* **87**, 64–80.

Lisle RJ, Styles P and Freeth SJ (1990) Fold interference structures: the influence of layer competence contrast. *Tectonophysics* **172**, 197–200.

McKenzie NR, Hughes NC, Myrow PM, Xiao S and Sharma M (2011) Correlation of Precambrian–Cambrian sedimentary successions across northern India and the utility of isotopic signatures of Himalayan lithotectonic zones. *Earth and Planetary Science Letters* **312**, 471–83.

Mishra DC, Singh B, Tiwari BM, Gupta SB and Rao MBSV (2000) Two cases of continental collisions and related tectonics during the Proterozoic period in India insights from gravity modeling constrained by seismic and magnetotelluric studies. *Precambrian Research* **99**, 149–69.

Passchier CW and Trouw RAJ (1998) *Microtectonics*. Berlin: Springer-Verlag.

Platt JP (1983) Progressive refolding in ductile shear zones. *Journal of Structural Geology* **5**, 619–22.

Prasad B (1984) Geology, sedimentation and paleogeography of the Vindhyan Supergroup, south-eastern Rajasthan. *Memoirs of the Geological Survey of India* **116**, 1–107.

Ramsay JG (1967) *Folding and Fracturing of Rocks*. New York: McGraw-Hill.

Ramsay JG and Huber MI (1983) *The Techniques of Modern Structural Geology, Vol. 1, Strain Analysis*. London: Academic Press, Inc. Ltd.

Ramsay JG and Huber MI (1987) *The Techniques of Modern Structural Geology, Vol. 2, Folds and Fractures*. London: Academic Press, Inc. Ltd.

Ray JS, Martin M, Veizer J and Bowring SA (2002) U-Pb zircon dating and Sr isotope systematics of the Vindhyan Supergroup, India. *Geology* **30**, 131–34.

Robin PYF and Cruden AR (1994) Strain and vorticity patterns in ideally ductile transpression zone. *Journal of Structural Geology* **16**, 447–66.

Roy AB and Kröner A (1996) Single zircon evaporation ages constraining the growth of Archean Aravalli craton, northwestern Indian shield. *Geological Magazine* **133**, 333–42.

Sahay A and Srivastava DC (2005a) Hour-glass structure: an evidence of buckle folding. *Journal of the Geological Society of India* **66**, 673–77.

Sahay A and Srivastava DC (2005b) Ductile shearing along the Great Boundary Fault: An example from the Berach river section, Chittaurgarh, Rajasthan. *Current Science* **88**, 557–60.

Sanderson DJ and Marchini WRD (1984) Transpression. *Journal of Structural Geology* **6**, 449–58.

Simonetti M, Carosi R, Montomoli C, Cottle JM and Iaccarino S (2020a) Timing and kinematics of flow in a transpressive dextral shear zone, Maures Massif (Southern France). *International Journal of Earth Sciences* **109**, 2261–85.

Simonetti M, Carosi R, Montomoli C, Cottle JM and Iaccarino S (2020b) Transpressive deformation in the Southern European Variscan Belt: new insights from the Aiguilles Rouges Massif (Western Alps) *Tectonics* **39**, 1–24.

Sinha-Roy S (2007) Evolution of Precambrian terrains and crustal-scale structures in Rajasthan craton, NW India. *International Association of Gondwana Research Memoir* **10**, 23–40.

Sinha-Roy S, Kirmani IR, Reddy BVR, Sahu RL and Patel SN (1986) Fold pattern of the Vindhyan sequence in relation to the Great Boundary Fault: example from Chittorgarh area, Rajasthan. *Quarterly Journal of the Geological, Mining and Metallurgical Society of India* **54**, 244–51.

Sinha-Roy S, Malhotra G and Mohanty M (1998) *Geology of Rajasthan*. Bangalore: Geological Society of India, 277 pp.

Sivaram TV and Odom AL (1982) Zircon geochronology of Berach granite of Chittorgarh, Rajasthan. *Journal of the Geological Society of India* **23**, 575–77.

Soto JI (1997) A general deformation matrix for three-dimensions. *Mathematical Geology* **29**, 93–130.

Srivastava DC, Lisle RJ and Vandycke S (1995) Shear zones as a new type of paleostress indicators. *Journal of Structural Geology* **17**, 663–76.

Srivastava DC and Sahay A (2003) Brittle tectonics and pore-fluid conditions in the evolution of the Great Boundary Fault around Chittaurgarh, Northwestern India. *Journal of Structural Geology* **25**, 1713–33.

Sylvester AG (1988) Strike-slip faults. *Geological Society of America Bulletin* **100**, 1666–703.

Tavarnelli E, Holdsworth RE, Klegg P, Jones RR and McCaffrey KJW (2004) The anatomy and evolution of a transpressional imbricate zone, Southern Uplands, Scotland. *Journal of Geology* **26**, 1341–60.

Tikoff TB and Fossen H (1993) Simultaneous pure and simple shear; the unifying deformation matrix. *Tectonophysics* **217**, 267–83.

Tikoff TB and Greene D (1997) Stretching lineations in transpressional shear zones: an example from the Sierra Nevada Batholith. *Journal of Structural Geology* **19**, 29–39.

Tikoff TB and Teyssier S (1997) Strain modelling of displacement-field partitioning in transpressional orogens. *Journal of Structural Geology* **16**, 1575–88.

Tiwari S (1995) Extension of the Great Boundary Fault (GBF) in the Ganga Valley. In *Continental Crust of Northwestern and Central India* (eds S Sinha-Roy and KR Gupta), pp. 311–28. Bangalore: Geological Society of India, Memoir no. 31.

Tobisch OT, Collerson KD, Bhattacharya T and Mukhopadhyay D (1994) Structural relationships and Sr-Nd isotope systematics in polymetamorphic granitic gneisses and granitic rocks from central Rajasthan, India: implications for the evolution of Aravalli craton. *Precambrian Research* **65**, 319–39.

Turner FH and Weiss LE (1963) *Structural Analysis of Metamorphic Tectonites.* New York: McGraw-Hill.

Valdiya KS (1998) The Aravalli-Himalayan connection. In *The Indian Precambrian* (ed. BS Paliwal), pp. 118–27. Jodhpur: Scientific Publishers, India.

Verma PK (1996) Evolution and age of the Great Boundary Fault of Rajasthan. *Memoirs of the Geological Society of India* **36**, 197–212.

Volpe AM and MacDougall JD (1990) Geochemistry and isotopic characteristics of mafic (Phulad Ophiolite) and related rocks in the Delhi Supergroup, Rajasthan, India: implications for rifting in the Proterozoic. *Precambrian Research* **48**, 167–91.

Wiedenbeck M and Goswami JN (1994) High precision $^{207}Pb/^{206}Pb$ zircon geochronology using a small ion microprobe. *Geochimica et Cosmochimica Acta* **58**, 2135–41.

Wiedenbeck M, Goswami JN and Roy AB (1996) Stabilisation of the Aravalli craton of north-west India at 2.5 Ga: an ion microprobe zircon study. *Chemical Geology* **129**, 325–40.

https://doi.org/10.1017/S0016756821000157 Published online by Cambridge University Press